An experimental test of the nicotinic hypothesis of COVID-19

Nicole E. Godellas[a] (ID), Gisela D. Cymes[a] (ID), and Claudio Grosman[a,b,c,1] (ID)

The pathophysiological mechanisms underlying the constellation of symptoms that characterize COVID-19 are only incompletely understood. In an effort to fill these gaps, a "nicotinic hypothesis," which posits that nicotinic acetylcholine receptors (AChRs) act as additional severe acute respiratory syndrome coronavirus 2 (SARS-CoV-2) receptors, has recently been put forth. A key feature of the proposal (with potential clinical ramifications) is the suggested competition between the virus' spike protein and small-molecule cholinergic ligands for the receptor's orthosteric binding sites. This notion is reminiscent of the well-established role of the muscle AChR during rabies virus infection. To address this hypothesis directly, we performed equilibrium-type ligand-binding competition assays using the homomeric human α7-AChR (expressed on intact cells) as the receptor, and radio-labeled α-bungarotoxin (α-BgTx) as the orthosteric-site competing ligand. We tested different SARS-CoV-2 spike protein peptides, the S1 domain, and the entire S1–S2 ectodomain, and found that none of them appreciably outcompete $[^{125}I]$-α-BgTx in a specific manner. Furthermore, patch-clamp recordings showed no clear effect of the S1 domain on α7-AChR–mediated currents. We conclude that the binding of the SARS-CoV-2 spike protein to the human α7-AChR's orthosteric sites—and thus, its competition with ACh, choline, or nicotine—is unlikely to be a relevant aspect of this complex disease.

SARS-CoV-2 | nicotinic receptors | acetylcholine receptors | spike protein | binding competition assays

According to official reports, as of August 2022, severe acute respiratory syndrome coronavirus 2 (SARS-CoV-2) has infected nearly 600 million people and caused more than 6.5 million deaths worldwide (1). According to recent estimates by the World Health Organization that aim to capture deaths missed by national reporting systems, however, the pandemic's true death toll is actually much higher: it amounts to ~15 million (2). Despite intensive research, our understanding of the pathophysiological mechanisms underlying the broad range of respiratory, neurological, psychiatric, and cardiovascular symptoms that follow this viral infection remains limited (3–7). Although the angiotensin-converting enzyme 2 (ACE2) was identified as the main cell-entry receptor (8–10), other plasma membrane receptors (such as neuropilin-1) (11, 12) and cell-surface glycocalyx components (such as heparan sulfate) (13) were also reported to participate in the different facets of this disease.

On the basis of amino acid sequence similarities between the SARS-CoV-2 spike protein and snake venom neurotoxins, it has recently been hypothesized that this coronavirus may also bind to nicotinic acetylcholine receptors (AChRs) (14–17). Moreover, it was suggested that the spike protein would bind to the receptor at a site that overlaps with the neurotransmitter-binding ("orthosteric") sites, in such a way that neurotoxins, the spike protein, and small-molecule cholinergic ligands would all bind to the receptor in a mutually exclusive, competitive manner. On the spike protein, the regions that were hypothesized to bind to AChRs map to two separate sequences: S^{375}TFKCYGVSPTKLNDL (S375–L390) (18), near the middle of the ACE2-binding domain (receptor-binding domain, RBD), and Y^{674}QTQTNSPRRAR (Y674–R685) (14), at the furin-cleavage site between domains S1 and S2 (Fig. 1). Remarkably, this bold proposal received ample support from molecular-simulation studies that led to the identification of putative interatomic interactions bridging the AChR–spike protein-binding interface (18, 19). Importantly, these simulations also suggested that the Y674–R685 stretch of amino acids remains accessible—and thus, fully competent to bind to the AChR—in the context of the fully glycosylated, full-length spike protein. Furthermore, the interaction between the receptor and the Y674–R685 spike protein peptide was found to be highly dependent on the AChR subtype, the peptide seemingly acting as an antagonist of the α4β2-AChR and the fetal-muscle-type AChR, and probably, as an agonist of the α7-AChR (19). These differences suggest that the extrapolation of experimental results obtained with one type of AChR to another one need not be valid, despite the highly similar binding modes of neurotoxins to muscle-type and α7-AChRs (20, 21).

Significance

Although much has been learned about the severe acute respiratory syndrome coronavirus 2 (SARS-CoV-2), the vast array of hitherto unexplained symptoms that characterize acute and postacute ("long") COVID-19 warrants the search for additional biochemical pathways involved. On the basis of amino-acid sequence analyses and computational approaches, it has recently been suggested that nicotinic acetylcholine receptors (AChRs) may act as additional SARS-CoV-2 plasma membrane receptors through the binding of the virus' spike protein to a site that overlaps with the orthosteric, ACh-binding sites. Here, on the basis of experimental ligand-binding competition assays, we conclude that the mutually exclusive binding of SARS-CoV-2 and cholinergic ligands to the human α7-AChR is unlikely to be a relevant aspect of this complex disease.

```
M¹FVFLVLLPLVSSQCVNLTTRTQLPPAYTNSFTRGVYYPDKVFR
SSVLHSTQDLFLPFFSNVTWFHAIHVSGTNGTKRFDNPVLPFNDG
VYFASTEKSNIIRGWIFGTTLDSKTQSLLIVNNATNVVIKVCEFQ
FCNDPFLGVYYHKNNKSWMESEFRVYSSANNCTFEYVSQPFLMDL
EGKQGNFKNLREFVFKNIDGYFKIYSKHTPINLVRDLPQGFSALE
PLVDLPIGINITRFQTLLALHRSYLTPGDSSSGWTAGAAAYYVGY
LQPRTFLLKYNENGTITDAVDCALDPLSETKCTLKSFTVEKGIYQ
TSNFRVQPTESIVRFPNITNLCPFGEVFNATRFASVYAWNRKRIS
NCVADYSVLYNSASFS³⁷⁵TFKCYGVSPTKLNDLCFTNVYADSFVI
RGDEVRQIAPGQTGKIADYNYKLPDDFTGCVIAWNSNNLDSKVGG
NYNYLYRLFRKSNLKPFERDISTEIYQAGSTPCNGVEGFNCYFPL
QSYGFQPTNGVGYQPYRVVVLSFELLHAPATVCGPKKSTNLVKNK
CVNFNFNGLTGTGVLTESNKKFLPFQQFGRDIADTTDAVRDPQTL
EILDITPCSFGGVSVITPGTNTSNQVAVLYQDVNCTEVPVAIHAD
QLTPTWRVYSTGSNVFQTRAGCLIGAEHVNNSYECDIPIGAGICA
SY⁶⁷⁴QTQTNSPRRAR▾SVASQSIIAYTMSLGAENSVAYSNNSIAI
PTNFTISVTTEILPVSMTKTSVDCTMYICGDSTECSNLLLQYGSF
CTQLNRALTGIAVEQDKNTQEVFAQVKQIYKTPPIKDFGGFNFSQ
ILPDPSKPSKRSFIEDLLFNKVTLADAGFIKQYGDCLGDIAARDL
ICAQKFNGLTVLPPLLTDEMIAQYTSALLAGTITSGWTFGAGAAL
QIPFAMQMAYRFNGIGVTQNVLYENQKLIANQFNSAIGKIQDSLS
STASALGKLQDVVNQNAQALNTLVKQLSSNFGAISSVLNDILSRL
DKVEAEVQIDRLITGRLQSLQTYVTQQLIRAAEIRASANLAATKM
SECVLGQSKRVDFCGKGYHLMSFPQSAPHGVVFLHVTYVPAQEKN
FTTAPAICHDGKAHFPREGVFVSNGTHWFVTQRNFYEPQIITTDN
TFVSGNCDVVIGIVNNTVYDPLQPELDSFKEELDKYFKNHTSPDV
DLGDISGINASVVNIQKEIDRLNEVAKNLNESLIDLQELGKYEQY
IKWPWYIWLGFIAGLIAIVMVTIMLCCMTSCCSCLKGCCSCGSCC
KFDEDDSEPVLKGVKLHYT
```

Fig. 1. Amino acid sequence of the spike protein of SARS-CoV-2 (GenBank: QHD43416.1). A PRRAR furin-cleavage site (a part of the Y674–R685 stretch, in cyan letters and underlined) separates the S1 domain from the S2 domain. The signal peptide is indicated with green letters; the ACE2-binding domain (RBD) is in orange; the S375–L390 stretch is in red and underlined; and the transmembrane segment is in magenta. The N terminus faces the extracellular milieu.

An interaction between the spike protein and AChRs could have pathological consequences not only because it could provide an alternative pathway for the virus to attach to and enter cells, but also because it could disrupt physiological AChR-mediated signaling. Moreover, the notion that the binding of the spike protein to the AChR is competitive with that of small-molecule cholinergic ligands would suggest a novel mechanism by which nicotine consumption and smoking-cessation drugs could affect the course of the disease (15–17, 22–24), the better understood mechanisms being the direct effect of nicotine and its analogs on the α7-AChR–mediated antiinflammatory response to viral infection (25–29).

However far-fetched these ideas may have seemed when first put forth, there is a well-known precedent: the rabies virus glycoprotein was reported to bind to the muscle-type (α1β1γδ) AChR in a manner that is mutually exclusive with the binding of α-bungarotoxin [a 74-amino acid neurotoxin from the Formosan banded krait; α-BgTx (30)] (31–35). This finding, along with other pieces of experimental evidence (e.g., refs. 36–38), has led to the well-established notion that the muscle AChR is one of the cell-attachment receptors for the rabies virus (39, 40). Quite notably, similar claims were made about the human-immunodeficiency virus-1 (HIV-1) glycoprotein 120 (gp120) and the muscle AChR (41, 42).

Given this background, the suggestion of a binding interaction between the SARS-CoV-2 spike protein and several AChRs (α1β1γδ, α4β2, α7, and α9) (14, 18, 19) seemed most intriguing and worth investigating experimentally. To this end, we performed equilibrium-type ligand-binding competition studies using the homomeric human α7-AChR (expressed on intact cells) as the receptor, and radio-labeled α-BgTx (at a concentration that half-saturates the α7-AChR) as the competing ligand.

We found that the two spike protein peptides (tested up to a concentration of ~250 μM), the S1 domain (~1.2 μM), and the entire S1–S2 ectodomain (~375 nM) fail to displace bound α-BgTx from this receptor to any appreciable degree. Furthermore, we found that the S1 domain (~20 nM) has no obvious effects on α7-AChR channel function. Thus, it seems inescapable to conclude that the binding of the SARS-CoV-2 spike protein to the human α7-AChR's orthosteric sites—and more specifically, the competition with ACh, choline, or nicotine for so doing—is unlikely to be a relevant aspect of this complex disease.

Results and Discussion

A most direct way of testing the "nicotinic hypothesis" of COVID-19 (14, 18, 19) is by means of competition ligand-binding assays. To this end, we followed a recently developed protocol for an equilibrium-type approach (43). To account for the likely importance of the membrane environment in the proposed ligand–receptor interactions, we used cell-surface-expressed AChRs, and to exclude the additional molecular players present in native systems [such as the lynx prototoxins expressed in neurons and immune cells (44), for example], we expressed AChRs heterologously on HEK-293 cells; indeed, only different AChRs and snake neurotoxins were used in the sequence alignments and molecular simulations that led to this hypothesis.

Briefly, HEK-293 cells transiently expressing the full-length, homomeric human α7-AChR were incubated in the presence of a constant concentration of $[^{125}I]$-α-BgTx and a variable concentration of unlabeled competing ligand for 24 or 48 h at 37 °C with constant rotation. The unlabeled and labeled ligands were added to the cells at nearly the same time. Enough toxin was used in the assays to ensure that the concentration of unbound ("free") $[^{125}I]$-α-BgTx was ~1 nM throughout each curve; this is the value of our estimate of the toxin's dissociation equilibrium constant from the α7-AChR's closed state at 37 °C ($K_{D,closed}$) (43). We previously found that, under these experimental conditions, the mixture of cell-expressed α7-AChRs, $[^{125}I]$-α-BgTx, and small-molecule cholinergic ligands (such as carbamylcholine, choline, or nicotine) approaches equilibrium closely (43). In the absence of competing unlabeled ligand, a 1-nM concentration of free $[^{125}I]$-α-BgTx ensures that approximately one-half of the toxin-binding sites on the receptor are occupied.

Fig. 2A shows concentration–response curves corresponding to the competition between $[^{125}I]$-α-BgTx and the S375–L390 peptide (Fig. 2A, cyan symbols). As its concentration rose into the hundreds of micromolar range, the S375–L390 peptide seemed to outcompete $[^{125}I]$-α-BgTx to some extent, but a quantitatively similar trend was observed when a scrambled peptide (that is, a peptide having the same amino acid composition but in a different sequence) was used, instead, as the unlabeled ligand (Fig. 2A, blue symbols). It may be argued that our assay was optimized for small-molecule ligands competing against $[^{125}I]$-α-BgTx and that longer incubations may be required when using peptides of the sort we used here. However, we found that unlabeled α-BgTx competed effectively against its radio-iodinated counterpart when incubated for 24 h at 37 °C (Fig. 2A). Indeed, the concentration of unlabeled toxin that displaced one-half of the bound $[^{125}I]$-α-BgTx was ~2.30 nM (Table 1), a value that is remarkably close to the theoretically expected value of ~2 nM (~2×$K_{D,closed}$) at equilibrium under the conditions of our experiments (43). On the other hand, the Hill coefficient (~1.25) (Table 1) was higher
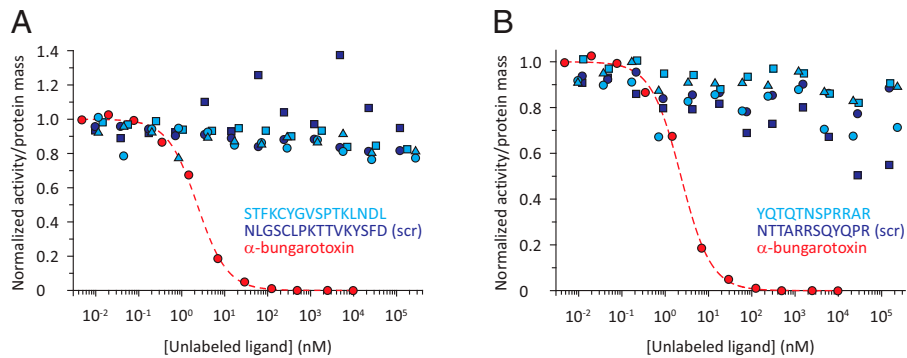
Fig. 2. Normalized concentration–response curves: competition between spike protein peptides and $[^{125}I]$-α-BgTx. Human α7-AChRs, $[^{125}I]$-α-BgTx, and unlabeled competing ligands were incubated at 37 °C for 24 or 48 h. Enough labeled toxin was used in the assays to ensure that the concentration of unbound $[^{125}I]$-α-BgTx was ∼1 nM throughout each curve. Hence, the ratio between the (fixed) concentration of free toxin and the toxin's K_D from the α7-AChR's closed state was approximately unity for all points of all curves. (*A*) S375–L390 peptide curve (cyan symbols). (*B*) Y674–R685 peptide curve (cyan symbols). For both panels, different symbol shapes denote different replicates of the same assay. Blue symbols correspond to competition assays that employed scrambled versions of each peptide as unlabeled ligands (sequence-specificity controls). Red symbols correspond to the competition between labeled and unlabeled α-BgTx (a positive control), and the dashed line corresponds to the fit with a single-component Hill equation (Table 1).

than the value of unity expected from an inverse agonist (43), such as α-BgTx (45, 46). It is likely that a somewhat longer incubation would have brought this system even closer to equilibrium, but in the context of this particular report, it is abundantly clear that 24-h incubations at 37 °C are long enough to detect the specific binding of short peptides to the α7-AChR.

Fig. 2*B* shows the concentration–response curves corresponding to the competition between $[^{125}I]$-α-BgTx and the Y674–R685 peptide (Fig. 2*B*, cyan symbols) and between $[^{125}I]$-α-BgTx and a scrambled peptide (Fig. 2, blue symbols). As was the case for S375–L390, some binding of the Y674–R685 peptide to the α7-AChR was observed in the concentration range tested, but inasmuch as a quantitatively similar effect was observed for a scrambled peptide, this binding was deemed not to be sequence-specific.

It is unclear what could have caused the small but clear displacement of bound $[^{125}I]$-α-BgTx in the presence of the highest concentrations of these four peptides, but we surmise that the presence of two lysines in S375–L390 and three arginines in Y674–R685 may have played a role. Certainly, under the conditions of our experiments, the binding of $[^{125}I]$-α-BgTx to the human α7-AChR is half-competed by a concentration as low as 11 μM of tetramethylammonium (TMA) (Table 1), a very small and simple organic cation (Fig. 3). Thus, arginines and protonated lysines in the context of short peptides could conceivably display some nonnegligible affinity for the α7-AChR, and possibly exert even some agonistic effect regardless of peptide sequence.

Fig. 3 shows concentration–response curves corresponding to the competition between $[^{125}I]$-α-BgTx and a variety of small-molecule cholinergic ligands, including the biologically relevant ACh, choline, and nicotine. Table 1 lists the corresponding half-competition concentrations and Hill coefficients. It is important to realize that these half-effective concentration values are not specific to $[^{125}I]$-α-BgTx acting as the competing ligand. Indeed, the same values would have been obtained for the competition against any other labeled antagonist or inverse agonist present at a concentration that half-saturates the receptor. It also seems important to emphasize that our failure to detect sequence-specific binding of the tested spike-protein peptides to the human α7-AChR is unlikely to be the result of the particular kinetics that their association to and dissociation from the receptor may have. Certainly, if these short (∼15-amino acid) peptides did bind to the human α7-AChR, they would most likely do so with kinetics that lie somewhere in-between those of the (slow) α-BgTx and the (fast) small-molecule cholinergic ligands. And, regardless of the extent to which chemical equilibrium was approached at the end of the incubations, both α-BgTx and the small-molecule ligands shown here outcompeted $[^{125}I]$-α-BgTx completely under the conditions of our experiments. It follows that our failure to detect sequence-specific binding of the tested spike-protein peptides results, in all likelihood, from their exceedingly low affinity for the human α7-AChR.

The undetectable affinity of the isolated S375–L390 and Y674–R685 peptides for the α7-AChR may result from their

Table 1. Half-competition concentrations and Hill-coefficient values for various cholinergic ligands binding to the human α7-AChR

Construct	Unlabeled ligand	Unlabeled-ligand half-competition concentration	Unlabeled-ligand n_H
Human α7-AChR	α-Bungarotoxin (1)	2.30 ± 0.18 nM	1.25 ± 0.09
	MLA (5)	88.9 ± 8.54 nM	0.95 ± 0.05
	Nicotine (3)	4.82 ± 0.24 μM	1.41 ± 0.06
	TMA (2)	11.4 ± 1.33 μM	1.46 ± 0.15
	ETMA (2)	15.6 ± 1.09 μM	1.66 ± 0.12
	ACh (1)	19.3 ± 1.51 μM	1.55 ± 0.13
	Carbamylcholine (4)	169 ± 9.30 μM	1.47 ± 0.07
	Choline (3)	204 ± 16.0 μM	1.28 ± 0.08
	DHβE (1)	472 ± 36.0 μM	1.03 ± 0.05

Binding-competition reactions against $[^{125}I]$-α-BgTx were incubated at 37 °C for 24 or 48 h. All individual curves for a given unlabeled ligand were globally fitted (regardless of incubation duration), and parameter SEs were obtained from these fits. The ratio between the fixed and half-saturation concentrations of $[^{125}I]$-α-BgTx was approximately unity. Parameter estimates are presented as mean ±1 SE. The number of independent assays contributing to each parameter estimation is indicated in parentheses.
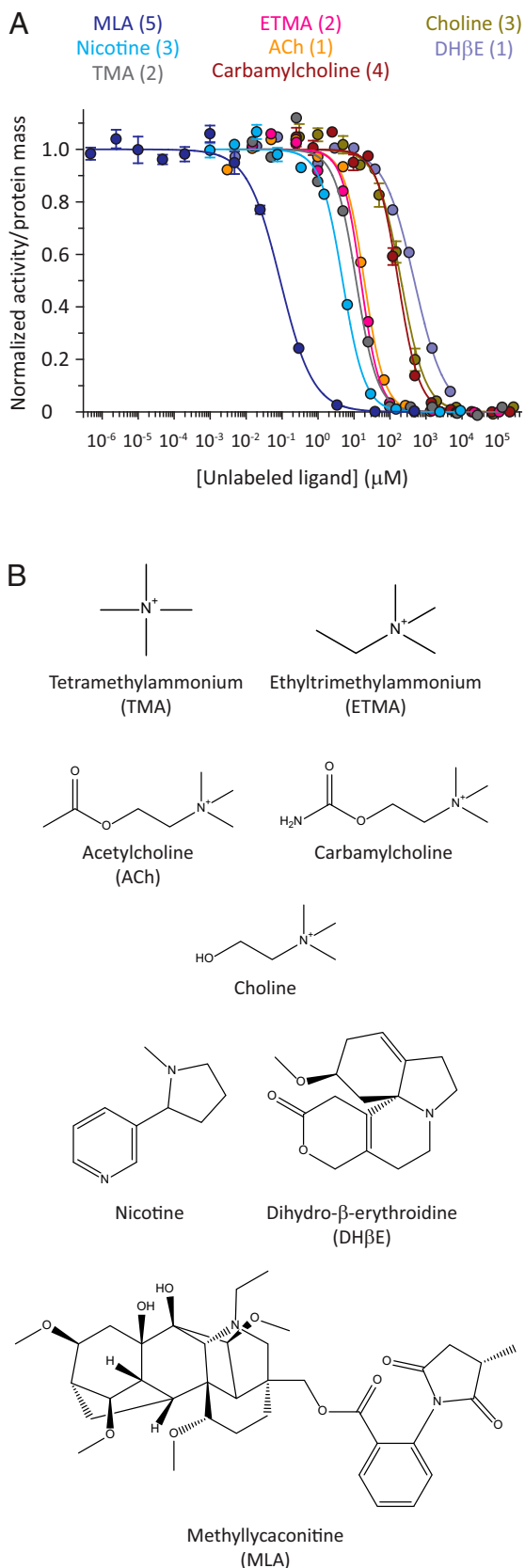
Fig. 3. Normalized concentration–response curves: competition between small-molecule AChR ligands and [^{125}I]-α-BgTx. Human α7-AChRs, [^{125}I]-α-BgTx, and unlabeled competing ligands were incubated at 37 °C for 24 or 48 h. Enough toxin was used in the assays to ensure that the concentration of unbound [^{125}I]-α-BgTx was ~1 nM throughout each curve. Hence, the ratio between the (fixed) concentration of free toxin and the toxin's K_D from the α7-AChR's closed state was approximately unity for all points of all curves. (A) Small-molecule cholinergic-ligand curves. The number of independent competition assays contributing to each plotted curve is indicated, in parentheses, in the corresponding figure caption; errors were calculated only when the latter was larger than 2. Error bars (±1 SE) smaller than the size of the symbols were omitted. The solid lines correspond to fits with single-component Hill equations (Table 1). Some of these curves (those corresponding to carbamylcholine, choline, nicotine, MLA, and DHβE) were reported elsewhere (43), and are reproduced here for the sake of comparison. (B) Structures of unlabeled ligands used in these experiments. Protonatable nitrogen atoms are shown in their deprotonated state.

inability to adopt the same conformation they assume in the intact protein (as was suggested for HIV's gp120 short peptides in their interaction with the human muscle AChR) (41). To account for this possibility, we also tested the effect of the entire S1 domain, from Gln-14 to Arg-685 (Fig. 1). A similar result was obtained, however: the binding of [^{125}I]-α-BgTx to the receptor was not outcompeted to any appreciable extent by ~1.2-μM S1 domain (a single, high concentration was used). Importantly, this domain contains both the S375-L390 and Y674-R685 peptides. For the sake of completeness, and to investigate the occurrence of interaction sites in the rest of the spike protein's extracellular portion, we also tested an uncleaved variant of the entire S1–S2 ectodomain (as a monomer). To prevent this protein fragment from being cleaved at the furin-cut site during biogenesis in HEK-293 cells, and to increase its stability as a soluble product, some mutations had to be introduced (*Materials and Methods*), including R682S and R685S, within the Y674-R685 stretch. At a concentration of ~375 nM (a single concentration was used), this S1–S2 ectodomain also failed to outcompete [^{125}I]-α-BgTx to any appreciable degree. To put things in quantitative perspective, the concentration at which this mutant form of the S1–S2 ectodomain half-saturates ACE2 has been reported to be ~1.7 nM (www.rndsystems.com; referred therein to as a "K_D"). Under the conditions of our experiments, a ligand with such an affinity for the human α7-AChR orthosteric sites would displace as much as one-half of the bound [^{125}I]-α-BgTx at a concentration of only ~3.4 nM (~2×$K_{D,closed}$). Other estimates of the affinity of the S1–S2 ecto-domain for ACE2, using different experimental approaches, confirm a value in the low nanomolar range (e.g., 3.8 nM in ref. 47). Evidently, the affinity of the tested spike protein peptides and fragments for the human α7-AChR's neurotransmitter-binding sites, if any, is several orders-of-magnitude lower.

Of note, whereas the S375-L390 amino acid stretch does not change in the B.1.617.2/Delta variant of concern (GenBank: QWK65230.1) and changes little in the B.1.1.529/Omicron variant (PDB ID code 7QO7; F^{375}TFKCYGVSPTKLNDL; the mutated residue is underlined), the Y674-R685 stretch changes in both, especially in Omicron (the sequence becomes Y^{674}QTQTNSRRRAR, in the Delta variant, and Y^{674}QTQTKSHGSAS, in the Omicron variant; mutated residues are underlined). Despite these mutations (some of which are extensive), these two variants remain highly infectious (48, 49).

Finally, having ruled out the competition between various segments of the spike protein and AChR ligands for binding to the human α7-AChR's orthosteric sites, we tested the effect of the S1 domain on channel function; to this end, we used whole-cell patch-clamp electrophysiology. We found that, when applied alone, the S1 domain (~20 nM) fails to elicit currents from α7-AChR–expressing HEK-293 cells. We also found that, when applied along with ACh ("coapplied") or when bathing the cells for up to 6 h before its coapplication with ACh ("preapplied"), this domain (~20 nM) fails to show a clear effect on the kinetics of currents activated by 100-μM ACh (Fig. 4). A similar insensitivity to the SARS-CoV-2 spike

protein has recently been reported for the currents mediated by the α3β4 AChR (50).

On the other hand, however, the Y674–R685 spike protein peptide has recently been reported to open human α7-AChRs in the presence of positive allosteric modulators (PAMs), but not in their absence (51). In addition to slowing down the kinetics of closed ⇌ open ⇌ desensitized state interconversions, PAMs stabilize the receptor channel's open and desensitized states (52–57). Thus, PAMs turn exceedingly low-efficacy agonists into agonists with detectable activity, much like many gain-of-function mutations do (e.g., refs. 45 and 58). Whether the agonistic effect of the Y674–R685 peptide (Y^{674}QTQTNSPRRAR) on the PAM-bound α7-AChR is sequence-specific or is merely the result of the presence of three positively charged arginines in its sequence (see our results, above, with the scrambled peptides), whether the effect is retained in the larger context of the entire spike protein, and where in the receptor the peptide-binding site responsible for this effect is located remain to be ascertained. Although it may be argued that the presence of a PAM in these experiments diminishes the physiological relevance of this finding, the observation is, nevertheless, quite intriguing.

Identifying the different membrane receptors a virus can bind to during an infection often proves challenging (e.g., refs. 35 and 59–62). Here, in order to test the nicotinic hypothesis of COVID-19 experimentally, we adopted a reductionist approach. We approximated α7-AChR–expressing neurons and immune cells with transiently transfected HEK-293 cells, and trimeric membrane-embedded spike proteins—which occur on the surface of SARS-CoV-2 virions at a density of 24 ± 9 trimers per particle (63)—with monomeric soluble peptides and protein fragments. Admittedly, we cannot completely rule out the possibility that these simplifications ended up weakening the interactions between the spike protein and the α7-AChR to the extent that we missed them altogether. Moreover, we cannot rule out the possibility that the full-length spike protein binds to the α7-AChR at a site that does not overlap with the neurotransmitter-binding sites, and that this binding has no appreciable effect on the currents activated by ACh. Finally, we did not address here the possibility that the spike protein binds to the orthosteric sites of the other AChRs (that is, α1β1γδ, α4β2, and α9) for which this interaction was also suggested on the basis of computational approaches (18, 19). Although, at this point, these alternative scenarios seem unlikely, further experiments that address these limitations are, undoubtedly, fully warranted.

Materials and Methods

cDNA Clones and Heterologous Expression. Complementary DNA (cDNA) coding the human α7-AChR (UniProt accession no. P36544) in pcDNA3.1 was purchased from addgene (#62276); cDNA coding isoform 1 of human RIC-3 [accession no. Q7Z5B4 (64)] in pcDNA3.1 was provided by W. N. Green, University of Chicago, IL; cDNA coding human NACHO [TMEM35A; accession no. Q53FP2 (65)] in pCMV6-XL5 was purchased from OriGene Technologies (#SC112910); cDNA coding the human acid-sensing ion channel subunit 1 (ASIC1; accession no. P78348) in pCR-BluntII-TOPO was purchased from horizon (#MHS6278-211689646) and was subcloned in pcDNA3.1; and cDNAs coding the mouse β1, δ, and ε subunits of the (muscle) AChR (accession nos. P09690, P02716, and P20782, respectively) in pRBG4 were provided by S. M. Sine, Mayo Clinic, Rochester, MN. The human α7-AChR was heterologously expressed in transiently transfected adherent HEK-293 cells grown at 37 °C and 5% CO_2. cDNAs coding the human α7-AChR, human RIC-3, and human NACHO were cotransfected using 125, 687.5, and 687.5 ng cDNA/cm^2, respectively; cDNA coding human ASIC1 was transfected using 187.5 ng cDNA/cm^2; and cDNAs coding the mouse β1-, δ-, and ε-AChR subunits were cotransfected using 62.5 ng cDNA/cm^2 each. Transfections were performed using a calcium-phosphate

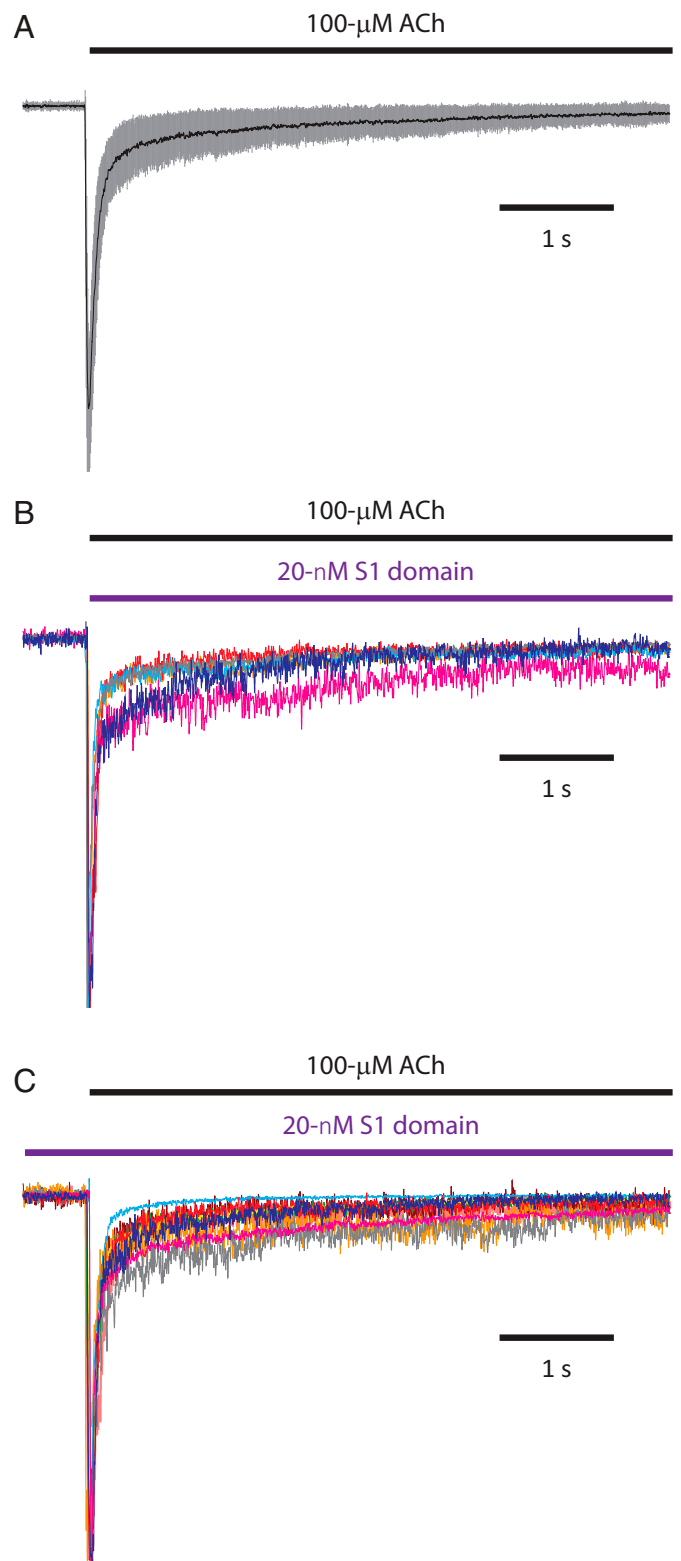**Fig. 4.** Exploring the effects of the SARS-CoV-2 spike protein S1 domain on human α7-AChR function. Inward currents were recorded at −60 mV in the whole-cell configuration upon changing the concentration of extracellular ACh and/or S1 domain. The currents were normalized to facilitate the visual comparison of their time courses. (*A*) The concentration of extracellular ACh was switched from 0 to 100 μM. Shown are the mean ±1 SD of 31 representative recordings obtained from 31 different cells. (*B*) The concentrations of extracellular ACh and S1 domain were switched from 0 to 100 μM and 20 nM, respectively. Shown are six representative recordings obtained from three different cells. (*C*) The concentration of extracellular ACh was switched from 0 to 100 μM. 20-nM S1 domain was present in the bath solution for up to several (up to 6) hours, as well as in both extracellular solutions flowing through the θ-tube applicator. Shown are 10 representative recordings obtained from 10 different cells.

precipitation method and proceeded for 16 to 18 h, after which the cell-culture medium (DMEM; Gibco) containing the DNA precipitate was replaced by fresh medium. As a control of the nonspecific binding of α-BgTx to transfected cells, HEK-293 cells were transiently transfected with cDNA coding human ASIC1 or the mouse β1-, δ-, and ε- (but not α1-) AChR subunits. These cells were incubated with [^{125}I]-α-BgTx (in the absence of unlabeled competitive ligand) under the same conditions as were the cells expressing the α7-AChR. The corresponding values of cell-bound radioactivity were used to normalize the competition curves (between 0 and 1) in those cases in which the highest concentrations of unlabeled ligand were unable to displace α7-AChR-bound [^{125}I]-α-BgTx completely.

Ligand-Binding Assays. Twenty-four hours after changing the cell-culture medium, transfected cells were resuspended in a Hepes-buffered sodium-saline solution (142 mM NaCl, 5.4 mM KCl, 1.8 mM CaCl$_2$, 1.7 mM MgCl$_2$, and 10 mM Hepes/NaOH, pH 7.4) by gentle agitation, and divided in 1-mL aliquots in 1.7-mL plastic tubes. Ligand-binding reaction mixtures were incubated at 37 °C for 24 or 48 h with constant rotation, and upon completion, cell-bound label was separated from unbound label by centrifugation at 16,000 × g for 3 min at room temperature. In order to reduce the amount of label bound nonspecifically to the cells, these pellets were resuspended in 1-mL of Dulbecco's phosphate-buffered saline (pH 7.4; Gibco), vortexed for 30 s, and pelleted again at 16,000 × g for 3 min at room temperature; this resuspension–pelleting procedure was repeated twice. Finally, the washed pellets were resuspended in a solution containing 0.1 N NaOH and 1% (wt/vol) sodium dodecyl sulfate (SDS), and incubated at 65 to 70 °C for 30 min. The radioactivity and protein content of each solubilized pellet were estimated: ^{125}I radioactivity was measured using a Wiper 100 γ-counter (Laboratory Technologies), and the amount of protein was measured using the bicinchoninic-acid assay (BCA; ThermoFisher) and a freshly prepared bovine serum albumin (ThermoFisher) calibration curve. The number of transfected cells contained in each reaction tube of any given curve was adjusted, by trial and error, so as to minimize the depletion of labeled and unlabeled ligands while ensuring a sufficiently high signal.

When ACh was used as the unlabeled ligand, the reaction mixtures also contained 2-μM paraoxon-ethyl (a cholinesterase inhibitor) to reduce the hydrolysis of ACh that would have otherwise occurred. The half-inhibitory concentration (IC$_{50}$) of this compound on the cholinesterase activity of red blood cells was reported to be in the ~75 to 90-nM range (66). The concentration of ACh for each point of the curve was estimated by measuring the corresponding concentration of choline present at the end of the 24-h incubation at 37 °C using a choline-oxidase–based colorimetric assay. The ACh–α-BgTx competition curve (Fig. 3A) was plotted against the calculated concentration of ACh; the concentration of choline in the mixture (10 to 20% of the initial ACh concentration) was ignored.

Most experiments were repeated several times, each one using two replicates per concentration of unlabeled ligand. Competition curves were fitted with single-component Hill equations using SigmaPlot 14 (Systat Software Products) and were normalized using the resulting parameters. When the number of replicates was larger than 1, all competition curves corresponding to a given unlabeled ligand were fitted globally. For display purposes, the data points corresponding to each replicate were normalized using the globally fitted parameters, averaged, and plotted as mean ±1 SE of the several replicates. For all fits, the reciprocal of the y axis variable was used as weight, and parameter SEs were computed using the reduced χ^2 statistic. [^{125}I]-α-BgTx was purchased from PerkinElmer (initial specific activity ≅ 80 to 140 Ci/mmol); MLA and DHβE were from Tocris Bioscience; ACh, carbamylcholine, choline, TMA, ETMA, nicotine, and paraoxon-ethyl were from Millipore-Sigma; SARS-CoV-2 spike protein peptides STFKCYGVSPTKLNDL and YQTQTNSPRRAR were from Genscript and JPT Peptide Technologies (each peptide was purchased from both companies and was assayed separately; no difference was found between the two sources); scrambled peptides NLGSCLPKTTVKYSFD and NTTARRSQYQPR were from Genscript; SARS-CoV-2 spike protein S1 domain (from Gln-14 to Arg-685) was from Genscript (#Z03501); SARS-CoV-2 spike protein ectodomain (from Val-16 to Lys-1211) containing mutations R682S and R685S (to eliminate the S1-S2 furin-cleavage site), K986P and V987P (to stabilize the prefusion state), and a C-terminal His tag was from R&D Systems (#10549-CV); and a choline-oxidase-based choline/ACh quantification colorimetric kit was from BioVision/abcam. The spike protein peptides (both wild-type and scrambled) were received lyophilized, resuspended in water, and stored at −80 °C until use; their concentrations were estimated spectrophotometrically at 280 nm using the corresponding calculated extinction coefficients. The spike protein S1 domain was received as a frozen solution and was stored at −80 °C until use. The spike protein S1-S2 ectodomain was received lyophilized, resuspended in phosphate-buffered saline solution, and stored at −80 °C until use.

Electrophysiology. Currents were recorded at ~22 °C with an effective bandwidth of DC–5 kHz using an Axopatch 200B amplifier (Molecular Devices), digitized at 100 kHz, and analyzed using pCLAMP 11.1 software (Molecular Devices). Series-resistance compensation was used and set to ~80%. The reference Ag/AgCl wire was connected to the extracellular solution through an agar bridge containing 200 mM KCl. Agonist-concentration jumps were applied to whole cells using a piece of double-barreled "θ-tubing" (Siskiyou). The flow of solution through the θ-tube was controlled using a gravity-fed system (ALA BPS-8; ALA Scientific Instruments), and the movement of the θ-tube was achieved using a piezo-electric arm (Burleigh-LSS-3100; discontinued) controlled by pCLAMP 11.1 software (Molecular Devices). The latter signals were low-pass–filtered (900C; Frequency Devices) at a cutoff frequency of 24.5 Hz prior to their arrival at the piezo-electric arm to reduce ringing in the θ-tube motion. During experiments, patched cells remained attached to a piece of collagen-coated glass coverslip (Neuvitro) placed at the bottom of the recording chamber. In this configuration, the perfusion system achieved a solution-exchange time of ~4 ms for the $t_{10-90\%}$ and ~10 ms for the $t_{90-10\%}$, as estimated from changes in the liquid-junction current measured with an open-tip patch pipette. The pipette solution was 110 mM KCl, 40 mM KF, and 5 mM Hepes/KOH, pH 7.4. The extracellular solution (flowing through the two barrels of a piece of θ-tubing) was 142 mM NaCl, 5.4 mM KCl, 1.8 mM CaCl$_2$, 1.7 mM MgCl$_2$, and 10 mM Hepes/NaOH, pH 7.4, with or without 100-μM ACh/~20-nM SARS-CoV-2 spike protein S1 domain. Patch pipettes, pulled from thin-walled borosilicate-glass capillary tubing (Sutter Instrument), had resistances of 3 to 5 MΩ when filled with pipette solution.

Data, Materials, and Software Availability. All study data are included in the article.

1. WHO, WHO Coronavirus (COVID-19) Dashboard. (2022) https://covid19.who.int/. Accessed 31 August 2022.
2. D. Adam, 15 million people have died in the pandemic, WHO says. *Nature* **605**, 206 (2022).
3. Z. Al-Aly, Mental health in people with covid-19. *BMJ* **376**, o415 (2022).
4. L. Bauer *et al.*, The neuroinvasiveness, neurotropism, and neurovirulence of SARS-CoV-2. *Trends Neurosci.* **45**, 358–368 (2022).
5. G. Douaud *et al.*, SARS-CoV-2 is associated with changes in brain structure in UK Biobank. *Nature* **604**, 697–707 (2022).
6. S. Spudich, A. Nath, Nervous system consequences of COVID-19. *Science* **375**, 267–269 (2022).
7. Y. Xie, E. Xu, B. Bowe, Z. Al-Aly, Long-term cardiovascular outcomes of COVID-19. *Nat. Med.* **28**, 583–590 (2022).
8. R. Gawish *et al.*, ACE2 is the critical in vivo receptor for SARS-CoV-2 in a novel COVID-19 mouse model with TNF- and IFNγ-driven immunopathology. *eLife* **11**, e74623 (2022).
9. M. Hoffmann *et al.*, SARS-CoV-2 cell entry depends on ACE2 and TMPRSS2 and is blocked by a clinically proven protease inhibitor. *Cell* **181**, 271–280.e8 (2020).
10. P. Zhou *et al.*, A pneumonia outbreak associated with a new coronavirus of probable bat origin. *Nature* **579**, 270–273 (2020).
11. L. Cantuti-Castelvetri *et al.*, Neuropilin-1 facilitates SARS-CoV-2 cell entry and infectivity. *Science* **370**, 856–860 (2020).
12. J. L. Daly *et al.*, Neuropilin-1 is a host factor for SARS-CoV-2 infection. *Science* **370**, 861–865 (2020).
13. T. M. Clausen *et al.*, SARS-CoV-2 infection depends on cellular heparan sulfate and ACE2. *Cell* **183**, 1043–1057.e15 (2020).
14. J.-P. Changeux, Z. Amoura, F. A. Rey, M. Miyara, A nicotinic hypothesis for Covid-19 with preventive and therapeutic implications. *C. R. Biol.* **343**, 33–39 (2020).
15. V. Dormoy *et al.*, Nicotinic receptors as SARS-CoV-2 spike co-receptors? *Med. Hypotheses* **158**, 110741 (2022).
16. K. Farsalinos *et al.*, Editorial: Nicotine and SARS-CoV-2: COVID-19 may be a disease of the nicotinic cholinergic system. *Toxicol. Rep.* **7**, 658–663 (2020).
17. K. Farsalinos, A. Barbouni, R. Niaura, Systematic review of the prevalence of current smoking among hospitalized COVID-19 patients in China: Could nicotine be a therapeutic option? *Intern. Emerg. Med.* **15**, 845–852 (2020).

18. K. Farsalinos *et al.*, Nicotinic cholinergic system and COVID-19: In silico identification of an interaction between SARS-CoV-2 and nicotinic receptors with potential therapeutic targeting implications. *Int. J. Mol. Sci.* **21**, E5807 (2020).

19. A. S. F. Oliveira *et al.*, A potential interaction between the SARS-CoV-2 spike protein and nicotinic acetylcholine receptors. *Biophys. J.* **120**, 983–993 (2021).

20. C. M. Noviello *et al.*, Structure and gating mechanism of the α7 nicotinic acetylcholine receptor. *Cell* **184**, 2121–2134.e13 (2021).

21. M. M. Rahman *et al.*, Structure of the native muscle-type nicotinic receptor and inhibition by snake venom toxins. *Neuron* **106**, 952–962.e5 (2020).

22. N. Alexandris *et al.*, Nicotinic cholinergic system and COVID-19: In silico evaluation of nicotinic acetylcholine receptor agonists as potential therapeutic interventions. *Toxicol. Rep.* **8**, 73–83 (2020).

23. G. Lagoumintzis *et al.*, Nicotinic cholinergic system and COVID-19: In silico identification of interactions between α7 nicotinic acetylcholine receptor and the cryptic epitopes of SARS-Co-V and SARS-CoV-2 Spike glycoproteins. *Food Chem. Toxicol.* **149**, 112009 (2021).

24. S. Tanmay, D. Labrou, K. Farsalinos, K. Poulas, Is SARS-CoV-2 spike glycoprotein impairing macrophage function via α7-nicotinic acetylcholine receptors? *Food Chem. Toxicol.* **152**, 112184 (2021).

25. L. V. Borovikova *et al.*, Vagus nerve stimulation attenuates the systemic inflammatory response to endotoxin. *Nature* **405**, 458–462 (2000).

26. A. Courties *et al.*, Regulation of the acetylcholine/α7nAChR anti-inflammatory pathway in COVID-19 patients. *Sci. Rep.* **11**, 11886 (2021).

27. J. Gonzalez-Rubio *et al.*, Cytokine release syndrome (CRS) and nicotine in COVID-19 Patients: Trying to calm the storm. *Front. Immunol.* **11**, 1359 (2020).

28. M. Kloc, R. M. Ghobrial, J. Z. Kubiak, How nicotine can inhibit cytokine storm in the lungs and prevent or lessen the severity of COVID-19 infection? *Immunol. Lett.* **224**, 28–29 (2020).

29. K. J. Tracey, The inflammatory reflex. *Nature* **420**, 853–859 (2002).

30. C. Y. Lee, Elapid neurotoxins and their mode of action. *Clin. Toxicol.* **3**, 457–472 (1970).

31. M. Gastka, J. Horvath, T. L. Lentz, Rabies virus binding to the nicotinic acetylcholine receptor alpha subunit demonstrated by virus overlay protein binding assay. *J. Gen. Virol.* **77**, 2437–2440 (1996).

32. T. L. Lentz, Rabies virus binding to an acetylcholine receptor alpha-subunit peptide. *J. Mol. Recognit.* **3**, 82–88 (1990).

33. T. L. Lentz, E. Hawrot, P. T. Wilson, Synthetic peptides corresponding to sequences of snake venom neurotoxins and rabies virus glycoprotein bind to the nicotinic acetylcholine receptor. *Proteins* **2**, 298–307 (1987).

34. T. L. Lentz, R. J. Benson, D. Klimowicz, P. T. Wilson, E. Hawrot, Binding of rabies virus to purified Torpedo acetylcholine receptor. *Brain Res.* **387**, 211–219 (1986).

35. T. L. Lentz, T. G. Burrage, A. L. Smith, J. Crick, G. H. Tignor, Is the acetylcholine receptor a rabies virus receptor? *Science* **215**, 182–184 (1982).

36. C. A. Hanham, F. Zhao, G. H. Tignor, Evidence from the anti-idiotypic network that the acetylcholine receptor is a rabies virus receptor. *J. Virol.* **67**, 530–542 (1993).

37. T. L. Lentz, P. T. Wilson, E. Hawrot, D. W. Speicher, Amino acid sequence similarity between rabies virus glycoprotein and snake venom curaremimetic neurotoxins. *Science* **226**, 847–848 (1984).

38. M. Rustici *et al.*, A monoclonal antibody to a synthetic fragment of rabies virus glycoprotein binds ligands of the nicotinic cholinergic receptor. *J. Mol. Recognit.* **2**, 51–55 (1989).

39. B. M. Davis, G. F. Rall, M. J. Schnell, Everything you always wanted to know about rabies virus (but were afraid to ask). *Annu. Rev. Virol.* **2**, 451–471 (2015).

40. M. Lafon, Rabies virus receptors. *J. Neurovirol.* **11**, 82–87 (2005).

41. L. Bracci, L. Lozzi, M. Rustici, P. Neri, Binding of HIV-1 gp120 to the nicotinic receptor. *FEBS Lett.* **311**, 115–118 (1992).

42. P. Neri, L. Bracci, M. Rustici, A. Santucci, Sequence homology between HIV gp120, rabies virus glycoprotein, and snake venom neurotoxins. Is the nicotinic acetylcholine receptor an HIV receptor? *Arch. Virol.* **114**, 265–269 (1990).

43. N. E. Godellas, C. Grosman, Probing function in ligand-gated ion channels without measuring ion transport. *J. Gen. Physiol.* **154**, e202213082 (2022).

44. J. M. Miwa, K. R. Anderson, K. M. Hoffman, Lynx prototoxins: Roles of endogenous mammalian neurotoxin-like proteins in modulating nicotinic acetylcholine receptor function to influence complex biological processes. *Front. Pharmacol.* **10**, 343 (2019).

45. S. Bertrand *et al.*, Paradoxical allosteric effects of competitive inhibitors on neuronal alpha7 nicotinic receptor mutants. *Neuroreport* **8**, 3591–3596 (1997).

46. M. B. Jackson, Spontaneous openings of the acetylcholine receptor channel. *Proc. Natl. Acad. Sci. U.S.A.* **81**, 3901–3904 (1984).

47. E. Cecon *et al.*, SARS-COV-2 spike binding to ACE2 in living cells monitored by TR-FRET. *Cell Chem. Biol.* **29**, 74–83.e4 (2022).

48. B. Meng *et al.*; CITIID-NIHR BioResource COVID-19 Collaboration; Genotype to Phenotype Japan (G2P-Japan) Consortium; Ecuador-COVID19 Consortium, Altered TMPRSS2 usage by SARS-CoV-2 Omicron impacts infectivity and fusogenicity. *Nature* **603**, 706–714 (2022).

49. P. Mlcochova *et al.*; Indian SARS-CoV-2 Genomics Consortium (INSACOG); Genotype to Phenotype Japan (G2P-Japan) Consortium; CITIID-NIHR BioResource COVID-19 Collaboration, SARS-CoV-2 B.1.617.2 Delta variant replication and immune evasion. *Nature* **599**, 114–119 (2021).

50. S. N. Grant, H. A. Lester, Regulation of epithelial sodium channel activity by SARS-CoV-1 and SARS-CoV-2 proteins. *Biophys. J.* **120**, 2805–2813 (2021).

51. J. F. Chrestia *et al.*, A functional interaction between Y674-R685 region of the SARS-CoV-2 spike protein and the human α7 nicotinic receptor. *Mol. Neurobiol.* **59**, 6076–6090 (2022).

52. J. K. Gill *et al.*, Agonist activation of α7 nicotinic acetylcholine receptors via an allosteric transmembrane site. *Proc. Natl. Acad. Sci. U.S.A.* **108**, 5867–5872 (2011).

53. J. H. Grønlien *et al.*, Distinct profiles of alpha7 nAChR positive allosteric modulation revealed by structurally diverse chemotypes. *Mol. Pharmacol.* **72**, 715–724 (2007).

54. R. S. Hurst *et al.*, A novel positive allosteric modulator of the alpha7 neuronal nicotinic acetylcholine receptor: In vitro and in vivo characterization. *J. Neurosci.* **25**, 4396–4405 (2005).

55. R. M. Krause *et al.*, Ivermectin: A positive allosteric effector of the alpha7 neuronal nicotinic acetylcholine receptor. *Mol. Pharmacol.* **53**, 283–294 (1998).

56. D. K. Williams, J. Wang, R. L. Papke, Investigation of the molecular mechanism of the α7 nicotinic acetylcholine receptor positive allosteric modulator PNU-120596 provides evidence for two distinct desensitized states. *Mol. Pharmacol.* **80**, 1013–1032 (2011).

57. G. T. Young, R. Zwart, A. S. Walker, E. Sher, N. S. Millar, Potentiation of alpha7 nicotinic acetylcholine receptors via an allosteric transmembrane site. *Proc. Natl. Acad. Sci. U.S.A.* **105**, 14686–14691 (2008).

58. C. Grosman, A. Auerbach, Asymmetric and independent contribution of the second transmembrane segment 12′ residues to diliganded gating of acetylcholine receptor channels: A single-channel study with choline as the agonist. *J. Gen. Physiol.* **115**, 637–651 (2000).

59. D. R. Castañeda-Castellanos, J. E. Castellanos, H. Hurtado, Differential use of the nicotinic receptor by rabies virus based upon substrate origin. *J. Neurovirol.* **8**, 150–154 (2002).

60. R. J. Ragotte *et al.*, Human Basigin (CD147) does not directly interact with SARS-CoV-2 spike glycoprotein. *MSphere* **6**, e0064721 (2021).

61. K. J. Reagan, W. H. Wunner, Rabies virus interaction with various cell lines is independent of the acetylcholine receptor. *Arch. Virol.* **84**, 277–282 (1985).

62. K. Wang *et al.*, CD147-spike protein is a novel route for SARS-CoV-2 infection to host cells. *Signal Transduct. Target. Ther.* **5**, 283 (2020).

63. Z. Ke *et al.*, Structures and distributions of SARS-CoV-2 spike proteins on intact virions. *Nature* **588**, 498–502 (2020).

64. M. Treinin, RIC-3 and nicotinic acetylcholine receptors: Biogenesis, properties, and diversity. *Biotechnol. J.* **3**, 1539–1547 (2008).

65. S. Gu *et al.*, Brain α7 nicotinic acetylcholine receptor assembly requires NACHO. *Neuron* **89**, 948–955 (2016).

66. F. A. Verdín-Betancourt *et al.*, In vitro inhibition of human red blood cell acetylcholinesterase (AChE) by temephos-oxidized products. *Sci. Rep.* **9**, 14758 (2019).